JACS
JOURNAL OF THE AMERICAN CHEMICAL SOCIETY

ARTICLE

pubs.acs.org/JACS

Ultrasound-Induced Emission Enhancement Based on Structure-Dependent Homo- and Heterochiral Aggregations of Chiral Binuclear Platinum Complexes

Naruyoshi Komiya, Takako Muraoka, Masayuki Iida, Maiko Miyanaga, Koichi Takahashi, and Takeshi Naota*

Department of Chemistry, Graduate School of Engineering Science, Osaka University, Machikaneyama, Toyonaka, Osaka 560-8531, Japan

Supporting Information

ABSTRACT: Instant and precise control of phosphorescent emission can be performed by ultrasound-induced gelation of organic liquids with chiral, clothespin-shaped *trans*-bis(salicylaldiminato)Pt(II) complexes, *anti*-**1**. Nonemissive solutions of racemic, short-linked *anti*-**1a** ($n = 5$) and optically pure, long-linked *anti*-**1c** ($n = 7$) in organic liquids are transformed immediately into stable phosphorescent gels upon brief irradiation of low-power ultrasound. Emission from the gels can be controlled by sonication time, linker length, and optical activity of the complexes. Several experimental results indicated that structure-dependent homo- and heterochiral aggregations and ultrasound-control of the aggregate morphology are key factors for emission enhancement.

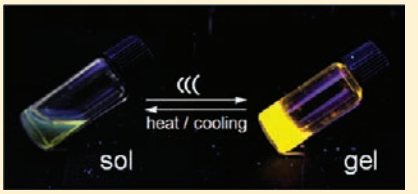

INTRODUCTION

A new method for photoluminescence (PL) control is required for the development of future technologies based on multipurpose chemical[1] and biological sensors[2] and light emitting devices.[3] In addition to conventional methods based on molecular transformation,[1,2,4] aggregation-based PL control has been explored extensively using a variety of chemical[5,6] and nonchemical stimuli.[7−10] Solvent-[5a−d] and additive-induced[5e,f] aggregation, thermal phase transition,[7] and vapochromism of crystals[6] are employed for this strategy. Mechanostress-induced disorder of self-quenched molecular aggregates has been recently studied as a new means to remotely control PL,[8] where the addition of piezo stimuli to nonemissive organometallic[8a−e] and organic[8f] crystals causes cleavage of metal−metal[8a−e] and π-stacking[8f] interactions, which leads to the recovery of their original phosphorescent properties. Single-bubble sonoluminescence is a unique phenomenon of piezo-responsive PL that occurs by the generation and collapse of cavitation during irradiation of high-power ultrasound.[9]

We report instant and switching emission enhancement based on ultrasound-induced aggregation[10,11] of potentially phosphorescent molecules. Nonemissive solutions of chiral, clothespin-shaped binuclear *trans*-bis(salicylaldiminato)Pt(II)[12] complexes doubly linked with polymethylene spacers (*anti*-**1**) undergo immediate linker-dependent hetero- and homochiral aggregation upon brief irradiation with low-power ultrasound to afford phosphorescent gel. The thermal reversibility, reproducibility, and ultrasound-controllability of the present sol−gel transition provides quick, remote, and precise OFF−ON control of emission by nonchemical stimuli. This paper describes the present phenomenon with focus on the ultrasound-induced gelation, dynamic photophysical change that occurs in these complexes, and its rationale with respect to the morphology and molecular arrays of the aggregates.

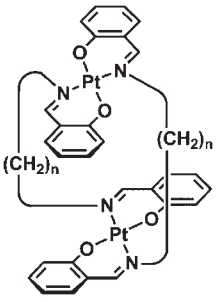

(+)-(*R*)-*anti*-**1**

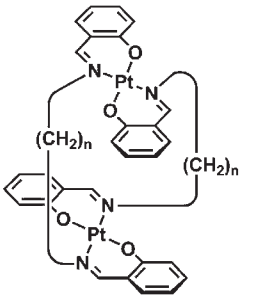

(−)-(*S*)-*anti*-**1** a: n = 5
b: n = 6
c: n = 7

RESULTS AND DISCUSSION

Synthesis and Structure of Binuclear Platinum Complexes. A series of platinum complexes, *anti*-**1a** ($n = 5$), *syn*-**1a** ($n = 5$), *anti*-**1b** ($n = 6$), *anti*-**1c** ($n = 7$), and *syn*-**1c** ($n = 7$), was prepared by reaction of $PtCl_2(CH_3CN)_2$ with the corresponding *N*,*N*′-bis(salicylidene)-1,ω-alkanediamine ($\omega = 5−7$) in boiling dimethyl sulfoxide (DMSO) and toluene. Achiral *syn* and racemic mixtures of chiral *anti* isomers were separated readily by silica gel column chromatography. Optically pure (100% ee) complexes, (+)-*anti*-**1a**, (−)-*anti*-**1a**, (+)-*anti*-**1c**, and (−)-*anti*-**1c**,

Received: April 28, 2011
Published: September 06, 2011

dx.doi.org/10.1021/ja2039369 | *J. Am. Chem. Soc.* 2011, 133, 16054–16061

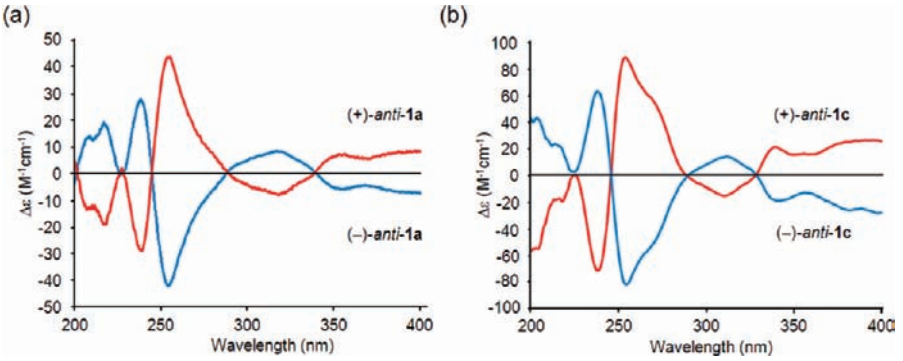

Figure 1. CD spectra of 1.00×10^{-5} M solutions of optically pure (a) *anti*-**1a** and (b) *anti*-**1c** in cyclohexane.

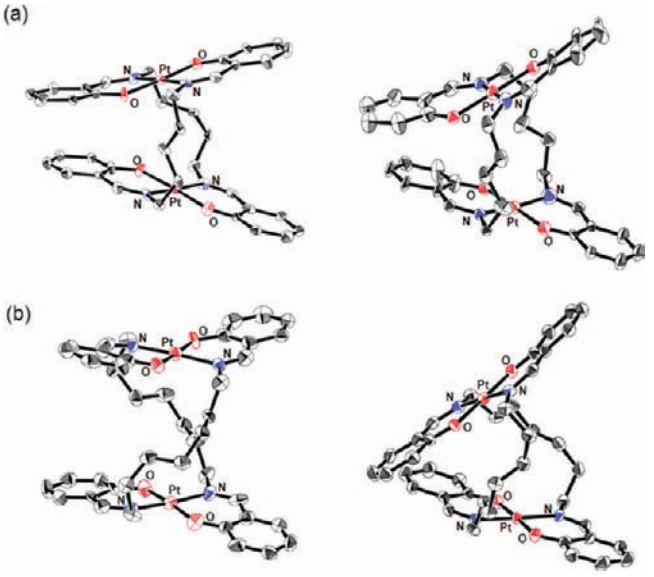

Figure 2. ORTEP representation of (a) (*R*)-*anti*-**1a** and (b) (*R*)-*anti*-**1c** as their racemic (left) and optically pure (right, (+)-form) crystals. Thermal ellipsoids are shown at the 50% probability level.

were obtained from the racemic mixtures using a preparative high performance liquid chromatography (HPLC) system with a chiral column. Circular dichroism (CD) spectra of these complexes in cyclohexane are shown in Figure 1.

Trans-coordination and *anti*-conformation in *anti*-**1a** and *anti*-**1c** have been unequivocally established by X-ray diffraction of their racemic and optically pure crystals obtained by recrystallization from ethyl acetate and cyclohexane, respectively (Figure 2). The molecular structures of (+)-*anti*-**1a** and (+)-*anti*-**1c** indicate that the absolute configuration of the (+)-form is *R*. As shown in four ORTEP representations, cofacial Pt coordination planes assume various 3D conformations with the help of flexible methylene linkers to achieve suitable molecular packing in their crystals. Such flexibility in these clothespin-shaped molecules would be a significant factor for a variety of morphological changes before and after sonication. The crystallographic data for racemic and optically pure *anti*-**1a** and *anti*-**1c** are listed in Table S1, Supporting Information.

Gelation Properties. The gelation properties of a series of **1** complexes were examined with and without ultrasonic irradiation of the solutions in various organic liquids (Table 1). Most solutions of **1** complexes do not form gels under conditions without sonicaton. Exceptionally, concentrated solutions of (±)-*anti*-**1a** in cyclohexane, cyclohexene, and benzene, and those of (+)-*anti*-**1c** in cyclohexane and cyclohexene spontaneously form gels, although slowly, when the solutions are allowed to stand at room temperature for 1 h without sonication. Irradiation of homogeneous solutions of (±)-*anti*-**1a** in various organic liquids with ultrasound waves (40 kHz, 0.45 W/cm^2, 10 s) gives the stable gels immediately after sonication, while (+)-*anti*-**1a** (100% ee) does not gelatinize any organic liquid, irrespective of the solution concentration and sonication time. This indicates that gelation with *anti*-**1a** proceeds in a heterochiral manner. *anti*-**1b** is entirely inert toward the gelation, but racemic and optically pure *anti*-**1c** exhibits high ultrasound-sensitivity for the gelation of various organic liquids. The minimum gelation concentrations of (±)-*anti*-**1a**, (±)-*anti*-**1c**, and (+)-*anti*-**1c** are given in Table 2. Various organic liquids, such as hydrocarbons, ethers, ketones, esters, and halogenated compounds can be gelatinized with a small amount of the gelator (0.1−1.9 wt % for (±)-*anti*-**1a**; 0.4−7.4 wt % for (±)-*anti*-**1c**; 0.3−7.4 wt % for (+)-*anti*-**1c**) immediately upon brief irradiation of low-power ultrasound. The sol−gel transition temperature (t_{gel}) of the ultrasound gels in cyclohexane (44 kHz, 0.31 W/cm^2, 10 s) was determined to be 63 °C for (±)-*anti*-**1a** (1.5×10^{-3} M), 47 °C for (±)-*anti*-**1c** (3.0×10^{-3} M), and 57 °C for (+)-*anti*-**1c** (3.0×10^{-3} M).

In contrast to *anti*-**1a**, the gelation ability of optically pure *anti*-**1c** was higher than that of the racemate (Tables 1 and 2). The time dependence of the concentration of nonaggregated monomer units was estimated by ^{1}H NMR analysis (500 MHz)[13] during the gelation of 1.80×10^{-3} M solutions of (±)-*anti*-**1c** and (+)-*anti*-**1c** in cyclohexane-d_{12} at 293 K upon sonication (44 kHz, 0.31 W/cm^2, 3 s) (Figure 3). The initial rate constants k_{obs} (k_{obs} = −d[(±)-*anti*-**1c**(nonaggregated)]/dt, −d[(+)-*anti*-**1c**-(nonaggregated)]/dt) were determined to be 1.64×10^{-6} and 3.85×10^{-7} M s^{-1}, respectively, which indicates that ultrasound-induced gelation with (+)-*anti*-**1c** proceeds 4.3 times faster than that with the (±)-form. These results imply that gelation with *anti*-**1c** proceeds by homochiral aggregation, and heterochiral association with the enantiomer acts as an inhibiting factor for gelation. This is a rare case of molecular aggregation where very slight differences in molecular structure significantly alter the association mode.

Ultrasound-Controlled Emission. All solutions of **1** in organic solvents did not exhibit significant emission under illumination of UV light; however, the ultrasound gels prepared from nonemissive, degassed solutions of (±)-*anti*-**1a**, (±)-*anti*-**1c**, and (+)-*anti*-**1c** did have intense yellow phosphorescent

dx.doi.org/10.1021/ja2039369 |*J. Am. Chem. Soc.* 2011, 133, 16054–16061

Table 1. Gelation Properties of 1 in Organic Liquids[a]

organic liquid	(±)-*anti*-**1a**	(+)-*anti*-**1a**	*syn*-**1a**	(±)-*anti*-**1b**	(±)-*anti*-**1c**	(+)-*anti*-**1c**	*syn*-**1c**
Cyclohexane	CG (CG)	P (P)	I (I)	P (P)	OG (OG)	OG (OG)	I (I)
Cyclohexene	OG (OG)	S (S)	I (I)	P (P)	OG (S)	OG (OG)	I (I)
Benzene	OG (OG)	S (S)	I (I)	P (P)	PG (S)	PG (S)	I (I)
Toluene	OG (S)	S (S)	I (I)	P (P)	PG (S)	PG (S)	I (I)
1,4-Dioxane	OG (S)	S (S)	I (I)	P (P)	S (S)	PG (S)	I (I)
Acetone	P (P)	S (S)	I (I)	P (P)	S (S)	OG (S)	I (I)
Ethyl acetate	P (P)	S (S)	I (I)	P (P)	S (S)	OG (S)	I (I)
CCl_4	OG (S)	S (S)	I (I)	P (P)	OG (S)	OG (S)	I (I)

[a] After sonication (40 kHz, 0.45 W/cm^2) of a 3.0 wt % solution of **1** in an organic liquid for 10 s at room temperature. Values in parentheses are those after standing at room temperature for 1 h without sonication. CG = clear gel, OG = opaque gel, PG = partial gel, P = precipitate, S = solution, I = partially insoluble.

Table 2. Minimum Gelation Concentration of 1[a]

	minimum gelation concentration (M × 10^3)		
organic liquid	(±)-*anti*-**1a**	(±)-*anti*-**1c**	(+)-*anti*-**1c**
Cyclohexane	0.7 (1.2)	3.0 (5.0)	2.2 (3.0)
Cyclohexene	4.3 (6.2)	7.9 (NG)	7.1 (13)
Benzene	6.1 (11)	51 (NG)	51 (NG)
Toluene	17 (NG)	61 (NG)	60 (NG)
1,4-Dioxane	13 (NG)	NG (NG)	39 (NG)
Acetone	NG (NG)	NG (NG)	24 (NG)
Ethyl acetate	NG (NG)	NG (NG)	23 (NG)
CCl_4	18 (NG)	18 (NG)	17 (NG)

[a] After sonication (40 kHz, 0.45 W/cm^2) for 10 s at room temperature. Values in parentheses are those after standing for 1 h at room temperature without sonication. NG: no gelation.

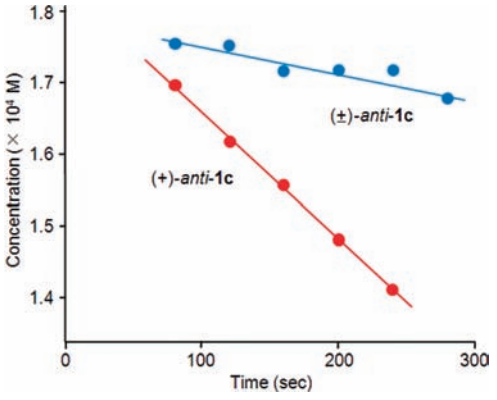

Figure 3. Time dependence over concentration of nonaggregated (+)-*anti*-**1c** and (±)-*anti*-**1c** in cyclohexane-d_{12} at 293 K after sonication (44 kHz, 0.31 W/cm^2, 3 s). Red data points: [(+)-*anti*-**1c**], $[(+)\text{-}anti\text{-}\mathbf{1c}]_0 = 1.80 \times 10^{-3}$ M, $k_{obs} = 1.64 \times 10^{-6}$ M s^{-1}, $R^2 = 0.994$; blue data points: [(±)-*anti*-**1c**], $[(\pm)\text{-}anti\text{-}\mathbf{1c}]_0 = 1.80 \times 10^{-3}$ M, $k_{obs} = 3.85 \times 10^{-7}$ M s^{-1}, $R^2 = 0.928$. Data were obtained from ^{1}H NMR (500 MHz) analysis in the range of 5.6–22% conversion of [(+)-*anti*-**1c**] and 2.6–6.7% conversion of [(±)-*anti*-**1c**].

emission. Figure 4 shows the emission properties of the solutions/gels of *anti*-**1a** and *anti*-**1c** in cyclohexane before and after sonication (44 kHz, 0.31 W/cm^2, 3 and 10 s). Significant changes

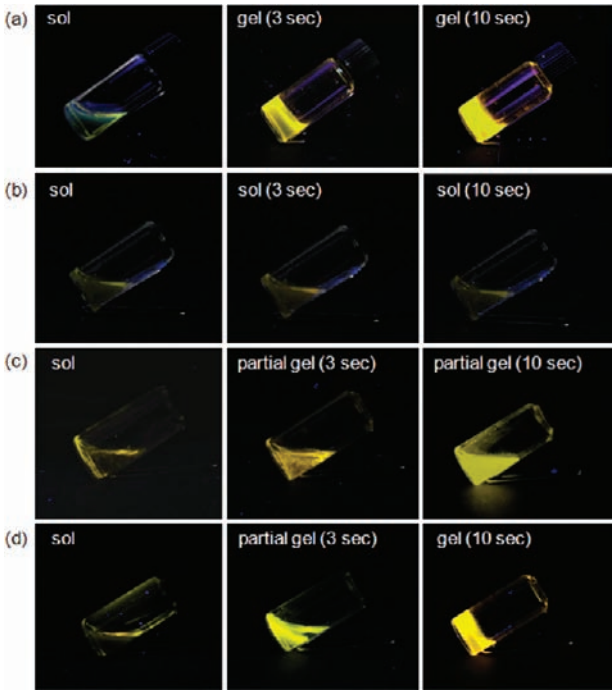

Figure 4. Emission properties of solutions/gels of (a) (±)-*anti*-**1a** (1.50×10^{-3} M), (b) (+)-*anti*-**1a** (1.50×10^{-3} M), (c) (±)-*anti*-**1c** (1.80×10^{-3} M), and (d) (+)-*anti*-**1c** (1.80×10^{-3} M) in cyclohexane. Photographs were taken before (left) and just after sonication (44 kHz, 0.31 W/cm^2) for 3 s (middle) and 10 s (right) under illumination at 365 nm.

in the fluidity and emission properties were observed upon sonication of the (±)-*anti*-**1a** solution (Figure 4a), while the (+)-*anti*-**1a** solution maintained a nonemissive sol state after sonication (Figure 4b). (±)-*anti*-**1c** did not gelatinize the solvent at such a low concentration, although there was a slight emission from the solution after sonication (Figure 4c). Nonemissive (+)-*anti*-**1c** solution emitted strongly after instant ultrasound-induced gelation (Figure 4d). The emissive gels thus formed were stable at ambient temperature, but were readily converted to the original nonemissive solution upon heating above a certain temperature, t_{gel}. The present OFF–ON switching emission can be repeated indefinitely with no measurable degradation of the gelator, because the emission arises from simple conformational changes of the complexes. The related nonreactive

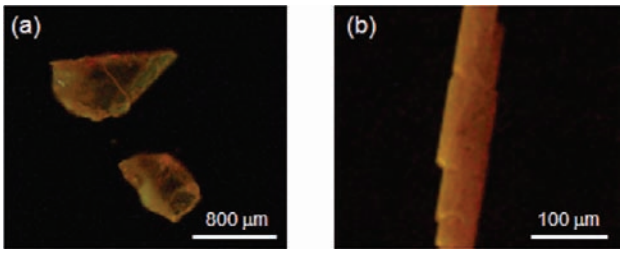

Figure 5. Optical microscope images of (a) (±)-*anti*-**1a** and (b) (+)-*anti*-**1c** crystals. Photographs were taken under illumination at 365 nm.

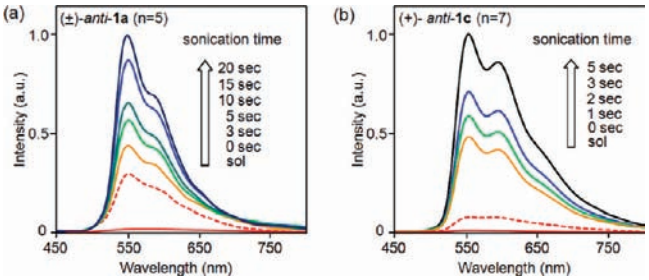

Figure 6. Emission spectra of gels of (a) (±)-*anti*-**1a** (1.50×10^{-3} M) and (b) (+)-*anti*-**1c** (2.20×10^{-3} M) in cyclohexane generated by sonication (44 kHz, 0.31 W/cm^2) for various irradiation times (λ_{ex} = 420 nm, 293 K). Dashed line: a spontaneous gel formed by standing at room temperature for 1 h without sonication.

complexes, such as *anti*-**1b**, all *syn* isomers, and noncyclic *trans*-bis(salicylaldiminato)platinum complexes, did not exhibit emission properties before or after sonication.

Notably, extended sonication yielded gels that exhibited more intensive emission, as shown in Figure 4a,c,d. Emission spectra for (±)-*anti*-**1a** and (+)-*anti*-**1c** gels in cyclohexane are shown in Figure 6. A significant increase in the maximum intensity at 551 nm ((±)-*anti*-**1a**) and 554 nm ((+)-*anti*-**1c**) was observed when the sonication time was prolonged from zero (solution) to 20 s. Similar OFF−ON switching profiles were observed in the gelation of a variety of organic liquids, such as benzene and 1,4-dioxane (Figure S1, Supporting Information). In each case, the relative emission intensity can be precisely controlled by tuning the sonication time. This controllability is rationally synchronized to a hyperchromic change in the metal-to-ligand charge transfer (MLCT) band at 450 nm (Figure S2, Supporting Information).

Figure 7 shows the dependence of the maximum emission intensity at 551−554 nm on the sonication time for solutions and gels of *anti*-**1a** and *anti*-**1c** under excitation at 420 nm. A strong, linear dependence on the sonication time was observed for the emission of (±)-*anti*-**1a** after ultrasound-induced gelation, while optically pure (+)-*anti*-**1a** did not exhibit emission enhancement, irrespective of the sonication time (Figure 7a). In contrast, the emission intensity and sonication sensitivity of (+)-*anti*-**1c** were much larger than those of the (±)-form (Figure 7b). Emission lifetimes (τ) of the ultrasound gels with (±)-*anti*-**1a** (1.50×10^{-3} M cyclohexane, 44 kHz, 0.31 W/cm^2, 3 s) and (+)-*anti*-**1c** (1.50×10^{-3} M cyclohexane, 44 kHz, 0.31 W/cm^2, 3 s) were determined to be 30, 137, 436 ns (44:48:8) and 21, 502 ns (75:25), respectively, by time-correlated single photon counting, which indicates that their yellow emissions are phosphorescent. The quantum yields of the gels at 77 K (Φ_{77K}) have been

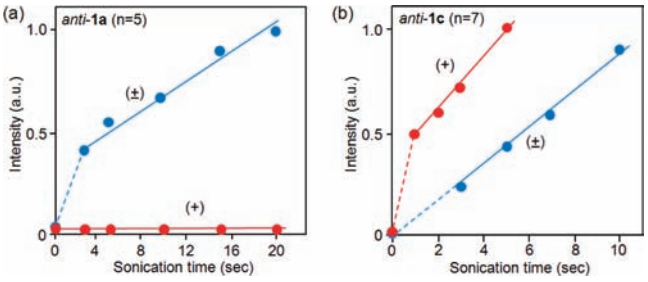

Figure 7. Maximum emission intensity of solutions/gels of (a) *anti*-**1a** (1.50×10^{-3} M, λ_{max} = 551 nm) and (b) *anti*-**1c** (2.15×10^{-3} M, λ_{max} = 554 nm) in cyclohexane as a function of sonication time (44 kHz, 0.31 W/cm^2) (λ_{ex} = 420 nm, 293 K). Blue data points, racemic compounds; red data points, (+)-forms (100% ee).

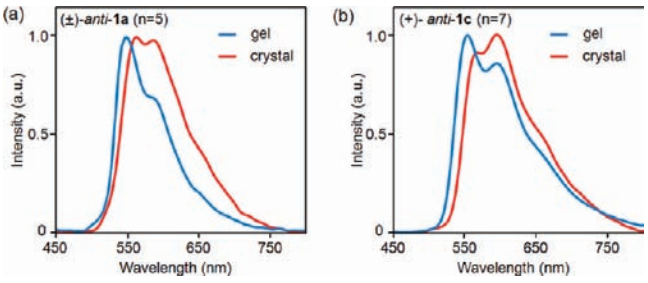

Figure 8. Normalized emission spectra of (a) (±)-*anti*-**1a** and (b) (+)-*anti*-**1c** (λ_{ex} = 420 nm, 293 K). Red lines, crystals; blue lines, ultrasound gels obtained from cyclohexane solutions (44 kHz, 0.31 W/cm^2).

determined to be 0.20 ((±)-*anti*-**1a**) and 0.34 ((+)-*anti*-**1c**) by the absolute method using an integrating sphere.[14]

It is noteworthy that a strong emission was observed exclusively after ultrasound-induced gelation. Figure 6 and Figure S1a (Supporting Information) show that no significant emission was observed for the spontaneous gels obtained from solutions of (±)-*anti*-**1a** and (+)-*anti*-**1c** in cyclohexane and benzene under nonsonication conditions. In addition, crystals of (±)-*anti*-**1a** and (+)-*anti*-**1c** obtained from ethyl acetate and cyclohexane, respectively, exhibited a weak orange emission under illumination at 365 nm as shown in the optical microscope images in Figure 5. Emissions of the crystals [λ_{max} = 563, 590 nm ((±)-*anti*-**1a**), 555, 601 nm ((+)-*anti*-**1c**)] were significantly red-shifted from those of the corresponding yellow ultrasound gels (Figure 8). Φ_{77K} values for the crystals were 0.048 and 0.16, which are lower than those of the cyclohexane gels.

Mechanistic Rationale for Ultrasound-Induced Gelation and Emission Enhancement. To elucidate the relevance of the emission properties in the ultrasound-induced gels, morphological change in the *anti*-**1** aggregates was examined using microscopic analysis. Figure 9 shows scanning electron microscopy (SEM) images of dried (±)-*anti*-**1a** samples obtained from solution and gel states. Large ca. 400 nm diameter nanoparticles were observed for the homogeneous solution of (±)-*anti*-**1a** in cyclohexane (Figure 9a). Colloidal aggregates in homogeneous solutions of *anti*-**1a** and *anti*-**1c** in cyclohexane were visually confirmed by clear Tyndall light scattering upon irradiation with a laser beam, as shown in Figure 10. The spherical morphology of the aggregates in colloidal solution is significantly different to the highly regulated, long and thin (ca. 50 nm wide) fibers after ultrasonic irradiation for 3 s (Figure 9b). Extended sonication

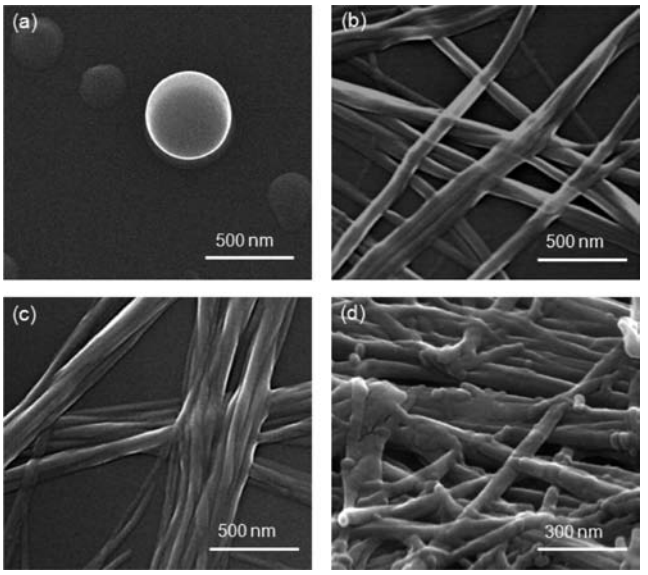

Figure 9. SEM images of dried (±)-*anti*-**1a** aggregates prepared from a 1.50×10^{-3} M solution in cyclohexane by various methods. (a) Solution prepared freshly; (b) gel just after brief sonication (44 kHz, 0.31 W/cm^2, 3 s); (c) gel just after extended sonication (44 kHz, 0.31 W/cm^2, 10 s); (d) gel formed spontaneously by standing at room temperature for 1 h without sonication.

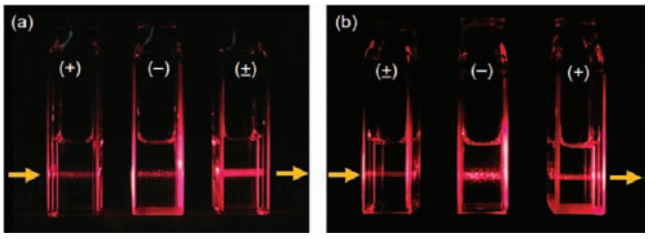

Figure 10. Photographs showing Tyndall scattering of a red laser beam, passing through 1.50×10^{-3} M solutions of racemic and optically pure (a) *anti*-**1a** and (b) *anti*-**1c** in ethyl acetate.

affords higher-order nanostructures consisting of flat bundles of the 50 nm fiber units (Figure 9c). Irregular, worm-like aggregates were observed on the spontaneous gel, which was obtained slowly by standing at room temperature without sonication (Figure 9d).

The molecular packing of racemic and optically pure *anti*-**1a** and *anti*-**1c** in their crystal states are shown in Figure 11. Homochiral interactions in (±)-*anti*-**1a** crystals, including cofacial interpenetrative stacking and Pt−Pt interactions, are major contributions to the molecular array of this A-shaped unit; however, heterochiral alignment of the linear homochiral sequence is also important as a specific supporting factor for close packing in crystals (Figure 11a). In contrast to strong intermolecular interactions in racemic crystals, very weak offset stacking interactions are observed in (+)-*anti*-**1a** crystals as a sole significant intermolecular factor for binding the optically pure units (Figure 11b). Interestingly, intermolecular interactions in racemic *anti*-**1c** crystals are much weaker than those in the optically pure (+)-form. H-shaped units in (±)-*anti*-**1c** crystals are packed with weaker Pt−Pt interactions (3.6 Å), while the A-shaped units of (+)-*anti*-**1c** are tightly bound to each other with a much stronger interaction (3.3 Å) (Figure 11c,d).

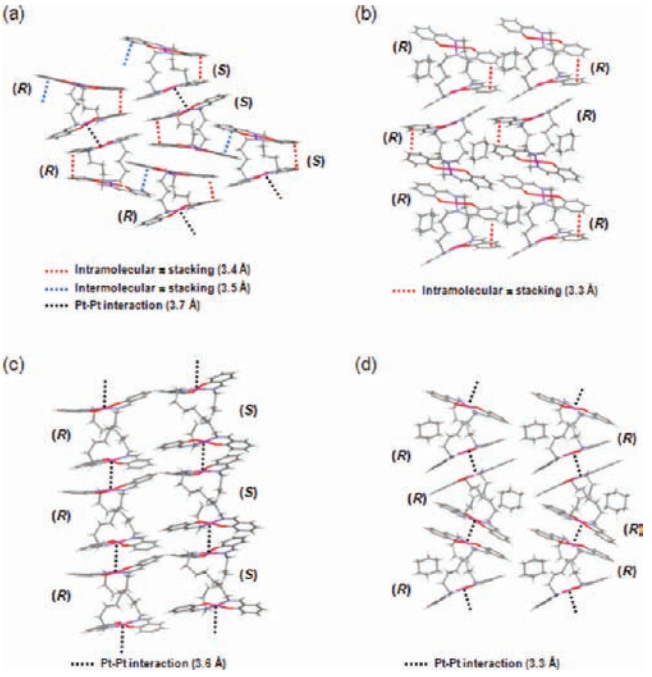

Figure 11. Packing of (a) (±)-*anti*-**1a**, (b) (+)-(*R*)-*anti*-**1a**·C_6H_{12}, (c) (±)-*anti*-**1c**, and (d) (+)-(*R*)-*anti*-**1c**·$2.5C_6H_{12}$ in the crystalline state.

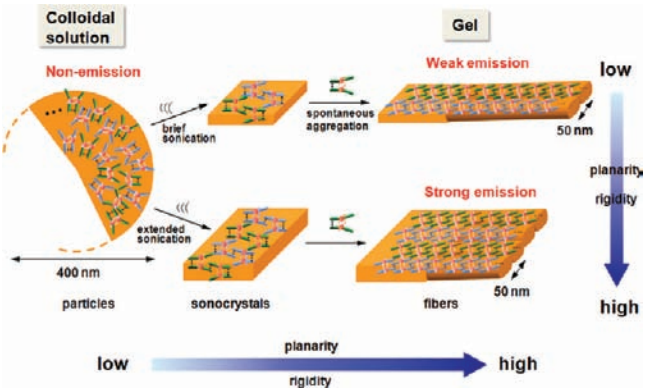

Figure 12. Schematic representation of the morphological and conformational change in aggregates during ultrasound-induced gelation for (±)-*anti*-**1a**.

On the basis of these experimental results, the present ultrasound-induced gelation can be rationalized by assuming the mechanism shown in Figure 12. *anti*-**1** forms colloidal particles in solution by loose, nonpenetrative, intermolecular stacking under nonsonication conditions. Imparting ultrasonic energy to the particles forms microcrystals[11c,15] that consist of interpenetrating molecular units similar to those presented in Figure 11. Given the similarity of the sonocrystals to the nonsonicated crystals, it seems reasonable to suppose that more robust (±)-*anti*-**1a** and (+)-*anti*-**1c** sonocrystals form exclusively as a stable growth core for aggregation under sonication. Further ultrasonication perturbs specific faces of the resulting sonocrystals to induce spontaneous anisotropic growth of flexible gel fibers. SEM observation of the aggregates with Pd analogues (*anti*-form, $n = 5$) revealed that platelet crystals are formed at the early stage of sonication, after which similar gel fibers of ca. 50 nm in width are propagated from the specific crystal faces.[16]

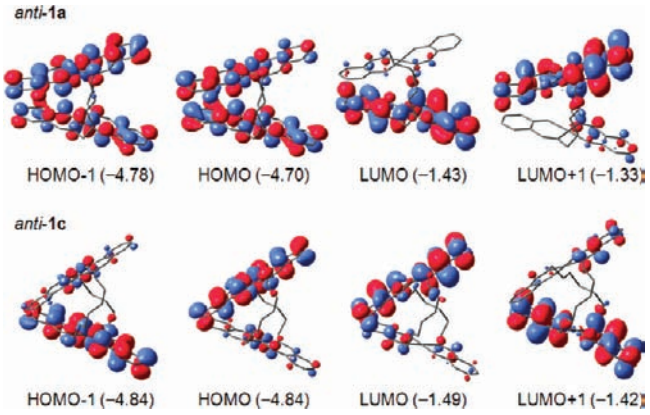

Figure 13. Plot of selected molecular orbitals and their eigenvalues (eV) for *anti*-**1a** and *anti*-**1c**, estimated by DFT calculations (B3LYP/6-31G*, LanL2DZ).

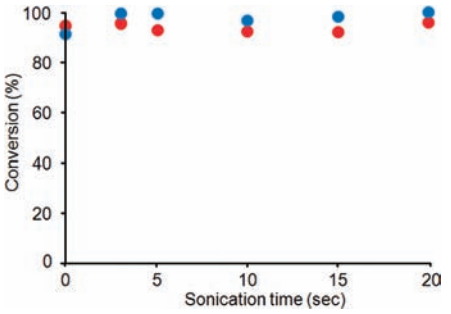

Figure 14. Relationship between conversion and sonication time (44 kHz, 0.31 W/cm^2) for gelation with (±)-*anti*-**1a** in cyclohexane-d_{12} (1.50×10^{-3} M) at 298 K. Conversions were determined by ^{1}H NMR (500 MHz) analysis of nonaggregated (±)-*anti*-**1a** (blue data points) and isolation of the gel fibers (aggregated (±)-*anti*-**1a**) by centrifugal separation (red data points).

Sonication of (±)-*anti*-**1a** solutions would afford a stable sonocrystal core, bearing heterochiral molecular alignment of strong homochiral interpenetrative stacking of optically pure *anti*-**1a** units, similar to the packing of (±)-*anti*-**1a** crystals (Figure 11a). The supposed heterochiral molecular alignment of the sonocrystal core would be inherited to the gel fibers, which would lead to heterochiral aggregation in the *anti*-**1a** gel. (+)-*anti*-**1a** does not form a sonocrystal core, due to instability of the packing structure of the crystal as supposed from weaker intermolecular interactions of the nonsonicated crystals (Figure 11b). Considering the contrasting stronger intermolecular interactions in (+)-*anti*-**1c** crystals (Figure 11d), sonication of (+)-*anti*-**1c** solutions would form a stable sonocrystal core that induces homochiral aggregation in the resulting gel fiber. It seems reasonable that a racemic mixture of *anti*-**1c** induces heterochiral conflict during homochiral aggregation, which leads to a retardation of the gelation process. Thus, we can be fairly certain that differences in the stabilization of growth cores of the gel fibers lead to the structurally dependent hetero- and homochiral aggregations during gelation with *anti*-**1a** and *anti*-**1c**. Although definitive information on the stacking modes of the propagation steps should wait for future investigation on the molecular structure of the gel fibers, we propose homochiral interpenetrative stacking of H-shaped units for short-linked (±)-*anti*-**1a** (Figure 12), and homochiral shuttlecock-type stacking[17] of A-shaped units for long-linked (+)-*anti*-**1c**, based on the packing structure of their crystals.

Density functional theory (DFT; B3LYP/6-31*G, LanL2DZ) calculations for *anti*-**1a** and *anti*-**1c** crystals showed that the HOMO and HOMO−1 are principally Pt(5d)−O(2p), while the LUMO and LUMO+1 are C═N (π^*) (Figure 13). Time dependent-DFT (TD-DFT) calculations indicated that the major electronic configuration of the $S_1(T_1)$ state is HOMO-to-LUMO (Tables S2 and S3, Supporting Information), which implies that the present phosphorescent emission is principally attributable to ^{3}MLCT. The nonemission properties of the colloidal particles, present under nonsonication conditions, can be rationalized by their loose, outward, noninterpenetrating molecular aggregation, which would allow sufficient mobility of the clothespin-shaped unit for nonradiative decay. Loose stacking of *anti*-**1** units in colloidal solutions is changed to rigid, inward stacking in gel fibers upon sonication, as shown in Figure 12. This morphological change causes significant decrease in the average mobility of each monomer unit, which leads to a suppression of energy loss for phosphorescent emission. The weak, red-shifted emissions of (±)-*anti*-**1a** and (+)-*anti*-**1c** crystals (Figures 5 and 8) can be ascribed to their close intra- and intermolecular contacts (Figures 11a and d), which induce strong donor−acceptor interactions and subsequent energy loss for emission.

It could simply be argued that the present emission enhancement is attributable to an increase in the sol−gel equilibrium constant, that is, an increase in the concentration of emissive, aggregated *anti*-**1** units with low mobility. To examine this possibility, the concentrations of nonaggregated *anti*-**1a** unit upon sonication for various times were estimated by ^{1}H NMR (500 MHz) analysis.[13] Conversions of (±)-*anti*-**1a** were determined to be constantly 92−99% for gelation of a 1.50×10^{-3} M solution in cyclohexane-d_{12} after sonication (40 kHz, 0.31 W/cm^2) for 3−10 s (blue data points in Figure 14). Such irreversibility of the gelation was also verified by centrifugal separation of the gel fibers, where aggregated *anti*-**1a** units were isolated in 92−96% yields from ultrasound gels produced by various sonication times (red data points in Figure 14). The results indicate that the ultrasound-induced emission enhancement of (±)-*anti*-**1a** is not attributable to an increase in the concentration of aggregated *anti*-**1a** units upon sonication, because all the monomer units are incorporated in the gel fibers, irrespective of the sonication time.

The significant increase in the absorbance of the MLCT band (Figure S2) upon extended sonication strongly suggests that emission enhancement occurs with increasing planarity of the coordination sites in the gel fibers. Thus, it is entirely fair to state that extended sonication enhances the average conformational fixation of almost all aggregation units of *anti*-**1a**. As shown in Figure 12, extended sonication would form larger crystalline nuclei with wider growth faces, from which highly bundled gel fibers (Figure 9c) are generated by subsequent spontaneous aggregation. This higher-ordered aggregation causes an increase in rigidity and decrease in mobility of each monomer unit, which would suppress the energy loss for phosphorescent emission. The irregular morphology of the spontaneous gel (Figure 9d), which can be ascribed to gradual generation of the growth core, would degrade the average emission ability of monomer unit due to the lower-order aggregations and random intermolecular contact. Research is currently underway to obtain definitive mechanistic information and to apply this new phenomenon to new stimuli-responsive emitting devices.

EXPERIMENTAL SECTION

General. Complexes **1** were prepared by reaction of $PtCl_2(CH_3CN)_2$ with the corresponding *N*,*N*′-bis(salicylidene)-1,ω-alkanediamine (ω = 5−7) in boiling DMSO and toluene. Optical resolution of (±)-*anti*-**1a** and (±)-*anti*-**1c** was performed using a Japan Analytical Industry Model LC-908 recycling preparative HPLC system with a Shiseido CD-Ph column (hexane/$CHCl_3$ = 1:1). Melting points were measured in a glass capillary on a Büchi B-545 melting point apparatus. IR spectra were recorded on a Bruker EQUINOX55/S spectrometer. Optical rotation was measured on a Jasco DIP-370 digital polarimeter. ^{1}H (Figures 3 and 14) and ^{13}C NMR spectra were recorded on a Varian Unity-Inova 500 spectrometer. CD spectra (Figure 1) were recorded on a Jasco J-805 spectropolarimeter. Ultrasonic irradiation was performed using a Honda HSR-301 sonoreactor (44 kHz, 0.31 W/cm^2, 14 × 14 × 14 cm vessel) and a Honda W-221 ultrasonic cleaner (40 kHz, 0.45 W/cm^2, 15 × 30 × 11 cm vessel). Optical micrographs (Figure 5) were taken with an Olympus BX41TF. Emission spectra (Figures 6−8 and Figure S1, Supporting Information) were obtained using a Jasco FP-6500 spectrometer. UV−vis spectra (Figure S2, Supporting Information) were obtained on a Shimadzu MultiSpec-1500 spectrometer. Quantum yields were measured by the absolute method using a JASCO FP-6500 spectrometer equipped with an integrating sphere. SEM images (Figure 9) were obtained on a Hitachi S-5000 L. Mass spectra were obtained on a JEOL JMS-DX 303.

***anti*-1a.** Orange solid (3.7%); mp 187−188 °C; IR (KBr): 2923, 2853, 1617, 1602, 1540, 1469, 1403, 1350, 1320, 1149, 1131, and 750 cm^{-1}; ^{1}H NMR ($CDCl_3$, 500 MHz): δ 7.65 (s, 4 H), 7.17 (ddd, *J* = 8.6, 7.3, 1.6 Hz, 4 H), 6.87 (dd, *J* = 7.3, 1.6 Hz, 4 H), 6.72 (br-d, *J* = 8.6 Hz, 4 H), 6.37 (ddd, *J* = 7.3, 7.3, 1.0 Hz, 4 H), 4.89 (ddd, *J* = 11.2, 7.0, 4.2 Hz, 4 H), 2.96 (ddd, *J* = 11.2, 5.3, 5.3 Hz, 4 H), 2.13 (ddd, *J* = 14.5, 7.3, 7.3 Hz, 4 H), and 1.85−2.00 (m, 8 H) ppm; ^{13}C NMR ($CDCl_3$, 125 MHz): δ 163.0, 159.0, 133.4, 133.0, 120.9, 119.6, 115.3, 56.6, 33.6, and 23.5 ppm; HRMS (FAB): *m*/*z* calcd for $C_{38}H_{40}N_4O_4{}^{195}Pt_2$ ([M]$^+$) 1006.2345, found 1006.2328. (+)-*anti*-**1a**: $[\alpha]_D{}^{22}$ = +167 ± 7 (*c* 0.036, $CHCl_3$). (−)-*anti*-**1a**: $[\alpha]_D{}^{26}$ = −167 ± 5 (*c* 0.021, $CHCl_3$).

***syn*-1a.** Orange solid (12%); mp 186−187 °C; IR (KBr): 2925, 2850, 1617, 1469, 1404, 1203, 1149, 1054, 956, and 749 cm^{-1}; ^{1}H NMR ($CDCl_3$, 500 MHz): δ 7.73 (s, 4 H), 7.12 (ddd, *J* = 7.9, 6.9, 2.0 Hz, 4 H), 7.00 (dd, *J* = 7.9, 2.0 Hz, 4 H), 6.68 (br-d, *J* = 7.9 Hz, 4 H), 6.37 (ddd, *J* = 7.9, 6.9, 1.0 Hz, 4 H), 4.93 (ddd, *J* = 11.2, 5.6, 5.6 Hz, 4 H), 2.87 (ddd, *J* = 11.2, 7.6, 3.6 Hz, 4 H), 2.11 (dddd, *J* = 14.4, 9.4, 4.7, 4.7 Hz, 4 H), 1.71−1.86 (m, 4 H), and 1.37−1.60 (m, 4 H) ppm; ^{13}C NMR ($CDCl_3$, 125 MHz): δ 163.3, 158.4, 133.3, 132.8, 120.3, 120.2, 115.1, 57.5, 32.1, and 22.7 ppm; HRMS (FAB): *m*/*z* calcd for $C_{38}H_{40}N_4O_4{}^{195}Pt_2$ ([M]$^+$) 1006.2345, found 1006.2343.

***anti*-1b.** Yellow solid (6.7%); mp > 291.0 °C (decomp.); IR (KBr): 2920, 2853, 1620, 1546, 1467, 1454, 1329, 1201, 1148, and 904 cm^{-1}; ^{1}H NMR ($CDCl_3$, 500 MHz): δ 7.77 (s, 4 H), 7.25 (ddd, *J* = 8.6, 6.9, 1.8 Hz, 4 H), 7.17 (dd, *J* = 7.9, 1.8 Hz, 4 H), 6.82 (br-d, *J* = 8.6 Hz, 4 H), 6.51 (ddd, *J* = 7.9, 6.9, 0.8 Hz, 4 H), 4.87 (ddd, *J* = 10.7, 6.5, 4.0 Hz, 4 H), 2.82 (ddd, *J* = 10.7, 10.7, 6.2 Hz, 4 H), 1.96−2.04 (m, 4 H), 1.74−1.83 (m, 4 H), 1.40−1.50 (m, 4 H), and 1.25−1.35 (m, 4 H) ppm; ^{13}C NMR ($CDCl_3$, 125 MHz): δ 164.0, 158.1, 133.43, 133.37, 120.7, 120.4, 115.3, 59.8, 31.7, and 26.6 ppm; MS (FAB) 1034.12 (M); HRMS (FAB): *m*/*z* calcd for $C_{40}H_{44}N_4O_4{}^{195}Pt_2$ ([M]$^+$) 1034.2658, found 1034.2673.

***anti*-1c.** Orange solid (10%); mp 256−257 °C; IR (KBr): 2922, 2850, 1620, 1601, 1541, 1469, 1451, 1355, 1324, 1206, 1147, 907, and 742 cm^{-1}; ^{1}H NMR ($CDCl_3$, 500 MHz): δ 7.59 (s, 4 H), 7.30 (ddd, *J* = 8.5, 7.1, 1.8 Hz, 4 H), 7.11 (dd, *J* = 7.9, 1.8 Hz, 4 H), 6.84 (br-d, *J* = 8.5 Hz, 4 H), 6.56 (ddd, *J* = 7.9, 7.1, 1.1 Hz, 4 H), 4.63 (ddd, *J* = 11.1, 6.9, 6.9 Hz, 4 H), 2.83 (ddd, *J* = 11.1, 6.8, 6.8 Hz, 4 H), 1.84−1.90 (m, 4 H), 1.41−1.70 (m, 12 H), and 1.20−1.30 (m, 4 H) ppm; ^{13}C NMR ($CDCl_3$, 125 MHz): δ 163.2, 158.7, 133.5, 133.4, 120.7, 120.3, 115.2, 57.5, 32.3, 28.1, and 25.6 ppm; HRMS (FAB): *m*/*z* calcd for $C_{42}H_{48}N_4O_4{}^{195}Pt_2$ ([M]$^+$) 1062.2971, found 1062.2977. (+)-*anti*-**1c**: $[\alpha]_D{}^{25}$ = +432 ± 4 (*c* 0.052, $CHCl_3$). (−)-*anti*-**1c**: $[\alpha]_D{}^{25}$ = −430 ± 4 (*c* 0.047, $CHCl_3$).

***syn*-1c.** Yellow solid (3.1%); mp > 280.0 °C (decomp.); IR (KBr): 2922, 2851, 1655, 1602, 1541, 1469, 1449, 1355, 1324, 1203, 1149, 905, and 752 cm^{-1}; ^{1}H NMR (DMSO-d_6, 500 MHz): δ 8.13 (s, 4 H), 7.32 (dd, *J* = 7.9, 1.8 Hz, 4 H), 7.10 (ddd, *J* = 8.6, 6.9, 1.8 Hz, 4 H), 6.69 (br-d, *J* = 8.6 Hz, 4 H), 6.45 (ddd, *J* = 7.9, 6.9, 0.9 Hz, 4 H), 4.43 (ddd, *J* = 11.0, 5.6, 5.6 Hz, 4 H), 3.07 (ddd, *J* = 11.0, 7.6, 7.6 Hz, 4 H), 1.61−1.70 (m, 8 H), and 1.26−1.50 (m, 12 H) ppm; HRMS (FAB): *m*/*z* calcd for $C_{42}H_{48}N_4O_4{}^{195}Pt^{196}Pt$ ([M]$^+$) 1063.2973, found 1063.2943.

X-ray Structure Determination. Crystals suitable for X-ray diffraction studies were analyzed using a Rigaku R-AXIS RAPID imaging plate diffractometer and a Rigaku Mercury 70 CCD diffractometer with graphite-monochromated Mo Kα radiation (λ = 0.71075 Å). The structures of (±)-*anti*-**1a**, (+)-*anti*-**1a**, (±)-*anti*-**1c**, and (+)-*anti*-**1c** were solved by direct methods and refined by the full-matrix least-squares method. In the subsequent refinement, the function $\Sigma\omega(F_o{}^2 - F_c{}^2)^2$, in which F_o and F_c are the observed and calculated structure factor amplitudes, respectively, was minimized. The positions of non-hydrogen atoms were found from difference Fourier electron density maps and refined anisotropically. All calculations were performed using Crystal Structure crystallographic software package, and illustrations were drawn by using ORTEP.[18] Details of the structure determinations are given in Figures 2, 11 and Table S1, Supporting Information.

Computational Methods. All calculations were carried out based on DFT with the B3LYP exchange-correlation functional,[19] using the Gaussian 09W program package.[20] The basis set used was the effective core potential (LanL2DZ) for platinum atoms[21] and 6-31G* for the remaining atoms.[22] Molecular orbitals and their eigenvalues for *anti*-**1** were calculated using the molecular geometries obtained from X-ray crystallographic analysis of (±)-*anti*-**1a** and (+)-*anti*-**1c**, respectively. The singlet−singlet ($E(S_n)$) and singlet−triplet ($E(T_n)$) transition energies were estimated by TD-DFT calculation (B3LYP/6-31G*, LanL2DZ).[23]

ASSOCIATED CONTENT

Supporting Information. Crystallographic data (Table S1), emission spectra (Figure S1), UV−vis spectra (Figure S2), TD-DFT calculation of major electric configuration (Tables S2 and S3) and complete ref 20. This material is available free of charge via the Internet at http://pubs.acs.org.

AUTHOR INFORMATION

Corresponding Author
naota@chem.es.osaka-u.ac.jp

ACKNOWLEDGMENT

This work was supported by a Grant-in-Aid for Scientific Research from the Japan Society for the Promotion of Science. We gratefully acknowledge Prof. Hiroshi Miyasaka and Assistant Prof. Syoji Ito (Osaka University) for conducting the lifetime measurements.

REFERENCES

(1) (a) Fletcher, N. C.; Lagunas, M. C. *Topics in Organometallic Chemistry*, Vol. 28. Springer-Verlag: Berlin, 2010; pp 143−170. (b) Quang, D. T.; Kim, J. S. *Chem. Rev.* **2010**, *110*, 6280–6301. (c) Lodeiro, C.; Capelo, J. L.; Mejuto, J. C.; Oliveira, E.; Santos, H. M.; Pedras, B.; Nuñez, C. *Chem. Soc. Rev.* **2010**, *39*, 2948–2976.

(2) (a) Wessels, J. T.; Yamauchi, K.; Hoffman, R. M.; Wouters, F. S. *Cytometry* **2010**, *77A*, 667–676. (b) Tomat, E.; Lippard, S. J. *Curr. Opin.*

Chem. Biol. **2010**, *14*, 225–230. (c) Duan, X.; Liu, L.; Feng, F.; Wang, A. S. *Acc. Chem. Res.* **2010**, *43*, 260–270. (d) Chan, C. P. *Bioanaysis.* **2009**, *1*, 115–133.

(3) (a) *Highly Efficient OLEDs with Phosphorescent Materials*; Yersin, H., Ed.; Wiley-VCH: Weinheim, 2008. (b) Chou, P.-T.; Chi, Y. *Chem.—Eur. J.* **2007**, *13*, 380–395.

(4) (a) Irie, M. *Chem. Rev.* **2000**, *100*, 1685–1716. (b) Hadjoudis, E.; Mavridis, I. M. *Chem. Soc. Rev.* **2004**, *33*, 579–588. (c) Cusido, J.; Deniz, E.; Raymo, F. M. *Eur. J. Org. Chem.* **2009**, 2031–2045.

(5) (a) Manimaran, B.; Thanasekaran, P.; Rajendran, T.; Lin, R.-J.; Chang, I.-J.; Lee, G.-H.; Peng, S.-M.; Rajagopal, S.; Lu, K.-L. *Inorg. Chem.* **2002**, *41*, 5323–5325. (b) An, B.-K.; Kwon, S.-K.; Jung, S.-D.; Park, S. Y. *J. Am. Chem. Soc.* **2002**, *124*, 14410–14415. (c) An, B.-K.; Gihm, S. H.; Chung, J. W.; Park, C. R.; Kwon, S.-K.; Park, S. Y. *J. Am. Chem. Soc.* **2009**, *131*, 3950–3957. (d) Hong, Y.; Lam, J. W. Y.; Tang, B. Z. *Chem. Commun.* **2009**, 4332–4353. (e) Leong, W. L.; Batabyal, S. K.; Kasapis, S.; Vittal, J. J. *Chem.—Eur. J.* **2008**, *14*, 8822–8829. (f) Chung, J. W.; Yoon, S.-J.; Lim, S.-J.; An, B.-K.; Park, S. Y. *Angew. Chem., Int. Ed.* **2009**, *48*, 7030–7034.

(6) Pt: (a) Buss, C. E.; Mann, K. R. *J. Am. Chem. Soc.* **2002**, *124*, 1031–1039. (b) Wadas, T. J.; Wang, Q.-M.; Kim, Y.-J.; Flaschenreim, C.; Blanton, T. N.; Eisenberg, R. *J. Am. Chem. Soc.* **2004**, *126*, 16841–16849. Au: (c) Mansour, M. A.; Connick, W. B.; Lachicotte, R. J.; Gysling, H. J.; Eisenberg, R. *J. Am. Chem. Soc.* **1998**, *120*, 1329–1330. (d) Rawashdeh-Omary, M. A.; Omary, M. A.; Fackler, J. P., Jr.; Galassi, R.; Pietroni, B. R.; Burini, A. *J. Am. Chem. Soc.* **2001**, *123*, 9689–9691. (e) Fernández, E. J.; López-de-Luzuriaga, J. M.; Monge, M.; Olmos, M. E.; Pérez, J.; Laguna, A.; Mohamed, A. A.; Fackler, J. P., Jr. *J. Am. Chem. Soc.* **2003**, *125*, 2022–2023. (f) Laguna, A.; Lasanta, T.; López-de-Luzuriaga, J. M.; Monge, M.; Naumov, P.; Olmos, M. E. *J. Am. Chem. Soc.* **2010**, *132*, 456–457.

(7) Liquid crystal phase: (a) Kozhevnikov, V. N.; Donnio, B.; Bruce, D. W. *Angew. Chem., Int. Ed.* **2008**, *47*, 6286–6289. Gel phase: (b) Huang, X.; Terech, P.; Raghavan, S. R.; Weiss, R. G. *J. Am. Chem. Soc.* **2005**, *127*, 4336–4344. (c) Kishimura, A.; Yamashita, T.; Aida, T. *J. Am. Chem. Soc.* **2005**, *127*, 179–183. (d) Strassert, C. A.; Chien, C.-H.; Galvez Lopez, M. D.; Kourkoulos, D.; Hertel, D.; Meerholz, K.; De Cola, L. *Angew. Chem., Int. Ed.* **2011**, *50*, 946–950. Crystal phase: (e) Sun, Y.; Ye, K.; Zhang, H.; Zhang, J.; Zhao, L.; Li, B.; Yang, G.; Yang, B.; Wang, Y.; Lai, S.-W.; Che, C.-M. *Angew. Chem., Int. Ed.* **2006**, *45*, 5610–5613. (f) Komiya, N.; Okada, M.; Fukumoto, K.; Jomori, D.; Naota, T. *J. Am. Chem. Soc.* **2011**, *133*, 6493–6496.

(8) Review: (a) Balch, A. L. *Angew. Chem., Int. Ed.* **2009**, *48*, 2641–2644. Au: (b) Lee, Y. A.; Eisenberg, R. *J. Am. Chem. Soc.* **2003**, *125*, 7778–7779. (c) Ito, H.; Saito, T.; Oshima, N.; Kitamura, N.; Ishizaka, S.; Hinatsu, Y.; Kato, M.; Tsuge, K.; Sawamura, M. *J. Am. Chem. Soc. 2008*, *130*, 10044−10045. Au−Ag: (d) Reference 6f. Cu: (e) Perruchas, S.; Le Goff, X. F.; Maron, S.; Maurin, I.; Guillen, F.; Garcia, A.; Gacoin, T.; Boilot, J.-P. *J. Am. Chem. Soc.* **2010**, *132*, 10967–10969. Pyrenes: (f) Sagara, Y.; Mutai, T.; Yoshikawa, I.; Araki, K. *J. Am. Chem. Soc.* **2007**, *129*, 1520–1521.

(9) Brenner, M. P.; Hilgenfeldt, S.; Lohse, D. *Rev. Mod. Phys.* **2002**, *74*, 425–484.

(10) Review: (a) Paulusse, J. M. J.; Sijbesma, R. P. *Angew. Chem., Int. Ed.* **2006**, *45*, 2334–2337. (b) Bardelang, D. *Soft Matter* **2009**, *5*, 1969–1971. (c) Cravotto, G.; Cintas, P. *Chem. Soc. Rev.* **2009**, *38*, 2684–2697.

(11) Organometallics: (a) Naota, T.; Koori, H. *J. Am. Chem. Soc.* **2005**, *127*, 9324–9325. (b) Isozaki, K.; Takaya, H.; Naota, T. *Angew. Chem., Int. Ed.* **2007**, *46*, 2855–2857. Peptides: (c) Bardelang, D.; Camerel, F.; Margeson, J. C.; Leek, D. M.; Schmutz, M.; Zaman, M. B.; Yu, K.; Soldatov, D. V.; Ziessel, R.; Ratcliffe, C. I.; Ripmeester, J. A. *J. Am. Chem. Soc.* **2008**, *130*, 3313–3315. (d) Xie, Z.; Zhang, A.; Ye, L.; Feng, Z. *Soft Mater* **2009**, *5*, 1474–1482. Aminoacids: (e) Li, Y.; Wang, T.; Liu, M. *Tetrahedron* **2007**, *63*, 7468–7473. (f) Wang, Y.; Zhan, C.; Fu, H.; Li, X.; Sheng, X.; Zhao, Y.; Xiao, D.; Ma, Y.; Ma, J. S.; Yao, J. *Langmuir* **2008**, *24*, 7635–7638. Ureas: (g) Wang, C.; Zhang, D.; Zhu, D. *J. Am. Chem. Soc.* **2005**, *127*, 16372–16373. (h) Baddeley, C.; Yan, Z.; King, G.; Woodward, P. M.; Badjić, J. D. *J. Org. Chem.* **2007**, *72*, 7270–7278. (i) Park, S. M.; Kim, B. H. *Soft Matter* **2008**, *4*, 1995–1997. (j) Yamanaka, M.; Fujii, H. *J. Org. Chem.* **2009**, *74*, 5390–5394. Choresterols: (k) Wu, J.; Yi, T.; Shu, T.; Yu, M.; Zhou, Z.; Xu, M.; Zhou, Y.; Zhang, H.; Han, J.; Li, F.; Huang, C. *Angew. Chem., Int. Ed.* **2008**, *47*, 1063–1067. (l) Dou, C.; Li, D.; Gao, H.; Wang, C.; Zhang, H.; Wang, Y. *Langmuir* **2010**, *26*, 2113–2118. Heterocycles: (m) Anderson, K. M.; Day, G. M.; Paterson, M. J.; Byrne, P.; Clarke, N.; Steed, J. W. *Angew. Chem., Int. Ed.* **2008**, *47*, 1058–1062. (n) He, Y.; Bian, Z.; Kang, C.; Jin, R.; Gao, L. *New J. Chem.* **2009**, *33*, 2073–2080. (o) Sambri, L.; Cucinotta, F.; De Paoli, G.; Stagni, S.; DeCola, L. *New J. Chem.* **2010**, *34*, 2093–2096.

(12) Static emission properties of bis(salicylaldiminato)Pt(II) complexes: *trans*-form (a) ref 7f. *cis*-form (b) Che, C.-M.; Kwok, C.-C.; Lai, S.-W.; Rausch, A. F.; Finkenzeller, W. J.; Zhu, N.; Yersin, H. *Chem.—Eur. J.* **2010**, *16*, 233–247.

(13) During the gelation, only nonaggregated monomer unit can be detected as ^{1}H NMR active signals because of their high molecular mobility in gel states. See, also: Frkanec, L.; Jokić, M.; Makarević, J.; Wolsperger, K.; Žinić, M. *J. Am. Chem. Soc.* **2002**, *124*, 9716–9717. (b) Miljanić, S.; Frkanec, L.; Meić, Z.; Žinić, M. *Langmuir* **2005**, *21*, 2754–2760.

(14) Kawamura, Y.; Sasabe, H.; Adachi, C. *Jpn. J. Appl. Phys.* **2004**, *43*, 7729–7730.

(15) Luque de Castro, M. D.; Priego-Capote, F. *Ultrason. Sonochem.* **2007**, *14*, 717–724.

(16) Komiya, N.; Hori, T.; Naota, T., unpublished result.

(17) Sawamura, M.; Kawai, K.; Matsuo, Y.; Kanie, K.; Kato, T.; Nakamura, E. *Nature* **2002**, *419*, 702–705.

(18) Burnett, M. N.; Johnson, C. K. *ORTEP-III: Oak Ridge Thermal Ellipsoid Plot Program for Crystal Structure Illustrations*, Report ORNL-6895; Oak Ridge National Laboratory: Oak Ridge, TN, 1996.

(19) Becke, A. D. *Modern Electronic Structure Theory Part II*; Yarkony, D. R., Ed.; World Scientific: Singapore, 1995.

(20) Frisch, M. J., et al. . *Gaussian 09*, Revision A.02; Gaussian, Inc.: Wallingford, CT, 2009.

(21) (a) Hay, P. J.; Wadt, W. R. *J. Chem. Phys.* **1985**, *82*, 270–283. (b) Hay, P. J.; Wadt, W. R. *J. Chem. Phys.* **1985**, *82*, 299–310.

(22) (a) Francl., M. M.; Pietro, W. J.; Hehre, W. J.; Binkley, J. S.; Gordon, M. S.; DeFrees, D. J.; Pople, J. A. *J. Chem. Phys.* **1982**, *77*, 3654–3665. (b) Hariharan, P. C.; Pople, J. A. *Theor. Chim. Acta* **1973**, *28*, 213–222.

(23) (a) Casida, M. E.; Jamorski, C.; Casida, K. C.; Salahub, D. R. *J. Chem. Phys.* **1998**, *108*, 4439–4449. (b) Stratmann, R. E.; Scuseria, G. E. *J. Chem. Phys.* **1998**, *109*, 8218–8224.